 CMES, vol.94, no.6, pp.485-505, 2013

Fast Boundary Knot Method for Solving Axisymmetric Helmholtz Problems with High Wave Number

J. Lin[1], W. Chen [1,2], C. S. Chen[3], X. R. Jiang[4]

Abstract: To alleviate the difficulty of dense matrices resulting from the boundary knot method, the concept of the circulant matrix has been introduced to solve axi-symmetric Helmholtz problems. By placing the collocation points in a circular form on the surface of the boundary, the resulting matrix of the BKM has the block structure of a circulant matrix, which can be decomposed into a series of smaller matrices and solved efficiently. In particular, for the Helmholtz equation with high wave number, a large number of collocation points is required to achieve desired accuracy. In this paper, we present an efficient circulant boundary knot method algorithm for solving Helmholtz problems with high wave number.

Keywords: boundary knot method, Helmholtz problem, circulant matrix, axisymmetric.

1 Introduction

The boundary knot method (BKM) [Chen and Tanaka (2002); Chen (2002); Chen and Hon (2003); Wang, Ling, and Chen (2009); Wang, Chen, and Jiang (2010); Zhang and Wang (2012); Zheng, Chen, and Zhang (2013)] has been widely applied for solving certain classes of boundary value problems. Instead of using the singular fundamental solution as the basis function in the method of fundamental solutions (MFS) [Fairweather and Karageorghis (1998); Fairweather, Karageorghis, and Martin (2003); Alves and Antunes (2005); Chen, Cho, and Golberg (2009); Drombosky, Meyer, and Ling (2009); Gu, Young, and Fan (2009); Lin, Gu, and Young (2010); Lin, Chen, and Wang (2011)], the BKM uses the non-singular general solution for the approximation of the solution. In the literature, both the MFS and BKM are classified as boundary-type meshless methods [Song and Chen

[1] College of Mechanics and Materials, Hohai University, Nanjing, P.R. China, 210098
[2] Corresponding to: chenwen@hhu.edu.cn
[3] Department of Mathematics, University of Southern Mississippi, USA
[4] Nanjing Les Information Technology Co.,Ltd, Nanjing, P.R. China, 210007

(2009); Chen, Lin, and Wang (2011); Tan, Zhang, Wang, and Miao (2011); Liu and Sarler (2013)]. In the MFS, the determination of the location of the source points on the fictitious boundary is a challenging issue. The major difference between the MFS and BKM is that no fictitious boundary is required for the BKM in the solution process. In terms of the numerical implementation, the BKM is much easier to implement than the MFS due to the use of general solutions rather than the fundamental solutions. In general, the BKM is applicable as long as the general solution of the underlying differential operator is known. Initially, the BKM had been used exclusively for solving homogeneous problems. However, recently the BKM has been applied to solve nonhomogeneous problems through the radial basis functions and the method of particular solutions [Golberg and Chen (Computational Mechanics Publications); Hon and Chen (2003); Lin, Chen, and Sze (2012); Mramor, Vertnik, and Sarler (2013)]. Since then, the BKM has been extended to solve a variety of physical problems governed by the Helmholtz, modified Helmholtz, Laplace, and the convection diffusion equations, including time-dependent problems and nonlinear problems [Jing and Zheng (2005a,b)]. Similar to the MFS, the resultant matrix of the BKM is dense and ill-conditioned [Li and Hon (2004); Liu (2008); Chen, Cho, and Golberg (2009)]. A direct solver for solving such matrices requires $O(N^3)$ operations and $O(N^2)$ memory storages. As such, there are not feasible for solving Helmholtz problems with high wave-number, where a large number of boundary collocation points is required. To our knowledge, the numerical efficiency of the BKM for solving these kinds of problems has not yet been published.

The purpose of this paper is to introduce a more efficient BKM for solving high wave number Helmholtz problems in axi-symmetric domain. The key idea behind this approach was inspired by the matrix decomposition algorithm in the literature of the MFS [Karageorghis and Fairweather (1998, 1999, 2000); Tsangaris, Smyrlis, and Karageorghis (2004, 2006); Karageorghis, Chen, and Smyrlis (2009)]. In general, the proposed algorithm decomposes the large system of equations into small linear systems of lower order. As in the traditional matrix decomposition method, the fast fourier transform (FFT) is crucial in augmenting the speed of computation.

2 The BKM formulation

Let Ω be a bounded open set in $\mathbb{R}^d, d = 2,3$, with boundary $\partial\Omega = \partial\Omega_D \cup \partial\Omega_N$ and $\partial\Omega_D \cap \partial\Omega_N = \emptyset$. In this paper we consider the following homogeneous Helmholtz problem

$$(\nabla^2 + k^2)u(\mathbf{x}) = 0, \qquad \mathbf{x} \in \Omega, \tag{1}$$

$$u(\mathbf{x}) = g_d(\mathbf{x}), \qquad \mathbf{x} \in \partial\Omega_D, \tag{2}$$

$$\frac{\partial u(\mathbf{x})}{\partial n} = g_n(\mathbf{x}), \qquad \mathbf{x} \in \partial\Omega_N, \tag{3}$$

where k is the wave number, and g_d and g_n are known functions.

Let $\{\mathbf{x}_j\}_{j=1}^N \in \partial\Omega$. The basic idea of the BKM is to approximate the solution of Eqs. (1)–(3) through a series of the general solutions ψ which are non-singular as follows:

$$u(\mathbf{x}) \simeq \tilde{u}(\mathbf{x}) = \sum_{j=1}^{N} \beta_j \psi(r_j) \tag{4}$$

where $r_j = \|\mathbf{x} - \mathbf{x}_j\|$ and $\|\cdot\|$ is the Euclidian norm. For the Helmholtz equation, we have [Chen (2002)]

$$\psi(r) = \begin{cases} J_0(kr), & \text{in 2D,} \\ \dfrac{\sin(kr)}{r}, & \text{in 3D.} \end{cases} \tag{5}$$

From Eqs. (2) and (3), by the collocation method, we have

$$\begin{aligned} &\sum_{j=1}^{N} \beta_j \psi(r_{ij}) = g_d(\mathrm{x}_i), \quad \mathbf{x}_i \in \partial\Omega_D, \\ &\sum_{j=1}^{N} \beta_j \frac{\partial \psi(r_{ij})}{\partial n} = g_n(\mathrm{x}_i), \quad \mathbf{x}_i \in \partial\Omega_N. \end{aligned} \tag{6}$$

Once the undetermined coefficient $\{\beta_j\}_{j=1}^N$ is obtained, the approximate solutions at any points can be obtained through Eq. (4).

3 Circulant matrix

To solve Eq. (6) using direct solver, one requires $O(N^3)$ operations, and $O(N^2)$ memory space, which is infeasible when the number of boundary collocation points becomes large. In this section, we briefly introduce the concept of the circulant matrix and the fast fourier transform to accelerate the solution process of an axi-symmetric domain.

Note that the resultant matrix from Eq. (6) is circulant if the solution domain is symmetric and the collocation points are uniformly distributed on the boundaries for two dimensional problems. The resultant matrix for the 3D case is somewhat different from the 2D case. Let $\mathbf{x}_{i,j} = \{(x_{i,j}, y_{i,j}, z_i)\}_{i=1,j=1}^{m,n}$ be the collocation points on the boundary. They are distributed in the following circular form on the surface of the boundary i.e.,

$$x_{i,j} = R_i \cos(\theta_j), \quad y_{i,j} = R_i \sin(\theta_j),$$

where

$$\theta_j = \frac{2\pi(j-1)}{n}, \quad j = 1, 2, \cdots, n.$$

Due to the axi-symmetry, the radius R_i of each concentreated circle is different for each z_i. At each height z_i, we have the same number of collocation points evenly distributed on a circle with radius R_i. From Eq. (6), we have

$$Q\beta = h \tag{7}$$

where

$$Q = \begin{pmatrix} Q_{11} & Q_{12} & \cdots & Q_{1m} \\ Q_{21} & Q_{22} & \cdots & Q_{2m} \\ \vdots & \vdots & \ddots & \vdots \\ Q_{m1} & Q_{m2} & \cdots & Q_{mm} \end{pmatrix}, \tag{8}$$

$$Q_{ij} = \begin{pmatrix} \psi(\|\mathbf{x}_{i1} - \mathbf{x}_{j1}\|) & \psi(\|\mathbf{x}_{i1} - \mathbf{x}_{j2}\|) & \cdots & \psi(\|\mathbf{x}_{i1} - \mathbf{x}_{jn}\|) \\ \psi(\|\mathbf{x}_{i2} - \mathbf{x}_{j1}\|) & \psi(\|\mathbf{x}_{i2} - \mathbf{x}_{j2}\|) & \cdots & \psi(\|\mathbf{x}_{i2} - \mathbf{x}_{jn}\|) \\ \vdots & \vdots & \ddots & \vdots \\ \psi(\|\mathbf{x}_{in} - \mathbf{x}_{j1}\|) & \psi(\|\mathbf{x}_{in} - \mathbf{x}_{j2}\|) & \cdots & \psi(\|\mathbf{x}_{in} - \mathbf{x}_{jn}\|) \end{pmatrix},$$

and

$$\beta = [\beta_1 \; \beta_2 \; \cdots \; \beta_{mn}]^T.$$

It is clear that Q_{ij} is formulated using the circular points on the i^{th} and j^{th} circles. Due to the symmetry, the sub-matrix Q_{ij} is circulant.

Before we proceed, we would like to give a brief review of the matrix decomposition of the circulant matrix. Let us consider the following $n \times n$ circulant matrix

$$M = circ(q_1, q_2, \cdots, q_n) \tag{9}$$

It is well-known that M can be decomposed as follows [Li and Hon (2004)]

$$M = U^* D U, \tag{10}$$

where

$$U^* = \frac{1}{\sqrt{n}} \begin{pmatrix} 1 & 1 & 1 & \cdots & 1 \\ 1 & w & w^2 & \cdots & w^{n-1} \\ 1 & w^2 & w^4 & \cdots & w^{2(n-1)} \\ \vdots & \vdots & \vdots & \ddots & \vdots \\ 1 & w^{n-1} & w^{2(n-1)} & \cdots & w^{(n-1)(n-1)} \end{pmatrix}, \tag{11}$$

and

$$D = diag(d_1, d_2, \cdots, d_n), \quad d_i = \sum_{k=1}^{n} q_k w^{(k-1)(i-1)}, \tag{12}$$

with $w = e^{2\pi i/n}$. Note that U is a unitary matrix i.e., $U^*U = UU^* = I$ and I is the identity matrix

Let $\otimes$ denote the matrix tensor product. The tensor product of a $m \times n$ matrix A and a $l \times k$ matrix B is defined as follows

$$A \otimes B = \begin{pmatrix} a_{11}B & a_{12}B & \cdots & a_{1n}B \\ a_{21}B & a_{22}B & \cdots & a_{2n}B \\ \vdots & \vdots & \ddots & \vdots \\ a_{m1}B & a_{m2}B & \cdots & a_{mn}B \end{pmatrix}$$

We also note that

$$(I_m \otimes U^*)(I_m \otimes U) = I_{mn}, \tag{13}$$

where I_m is the $m \times m$ identity matrix.

Pre-multiplying Eq. (7) by the block diagonal $mn \times mn$ matrix $I_m \otimes U$ and using the fact that U is unitary, we have

$$(I_m \otimes U)Q(I_m \otimes U^*)(I_m \otimes U)\alpha = (I_m \otimes U)f. \tag{14}$$

From the above equation, it follows that

$$\bar{Q}\bar{\alpha} = \bar{f}, \tag{15}$$

where

$$\begin{aligned} \bar{Q} = (I_m \otimes U)Q(I_m \otimes U^*) &= \begin{pmatrix} UQ_{11}U^* & UQ_{12}U^* & \cdots & UQ_{1m}U^* \\ UQ_{21}U^* & UQ_{22}U^* & \cdots & UQ_{2m}U^* \\ \vdots & \vdots & \ddots & \vdots \\ UQ_{m1}U^* & UQ_{m2}U^* & \cdots & UQ_{mm}U^* \end{pmatrix} \\ &= \begin{pmatrix} D_{11} & D_{12} & \cdots & D_{1m} \\ D_{21} & D_{22} & \cdots & D_{2m} \\ \vdots & \vdots & \ddots & \vdots \\ D_{m1} & D_{m2} & \cdots & D_{mm} \end{pmatrix}. \end{aligned} \tag{16}$$

and

$$\bar{\alpha} = (I_m \otimes U)\alpha, \tag{17}$$

$$\bar{f} = (I_m \otimes U) f. \tag{18}$$

In Eq. (16), each of the $n \times n$ block matrix D_{kl} is diagonal. In particular, if the sub-matrix of Q in Eq. (8) is circulant, i.e.,

$$Q_{ij} = circ(q_1, q_2, \cdots, q_n) = \begin{pmatrix} q_1 & q_2 & \cdots & q_n \\ q_n & q_1 & \cdots & q_{n-1} \\ \cdots & \cdots & \vdots & \cdots \\ q_2 & q_3 & \cdots & q_1 \end{pmatrix}, \tag{19}$$

then $D_{ij} = diag(d_{i,j}^1, d_{i,j}^2, \cdots, d_{i,j}^n)$ where

$$d_{i,j}^l = \sum_{k=1}^{n} q_k w^{(k-1)(l-1)}, \quad l = 1, 2, \cdots, n. \tag{20}$$

Since the matrix Q in Eq. (7) has been decomposed into m^2 blocks of the order n diagonal matrices, Eq. (15) can be decomposed into solving n systems of order m; i.e.,

$$E_l \alpha_l = \bar{f}_l, \quad l = 1, 2, \cdots, n, \tag{21}$$

where

$$\begin{aligned} (E_l)_{ij} &= d_{i,j}^l, \quad i, j = 1, 2, \cdots, m, \quad l = 1, 2, \cdots, n, \\ (\bar{f}_l)_i &= (\bar{f})_{(i-1)n+l}, \quad i = 1, 2, \cdots, m, \quad l = 1, 2, \cdots, n. \end{aligned} \tag{22}$$

We can summarize the above procedures in the following matrix decomposition algorithm:

`Step I.` Transform the right hand vector by $\bar{f} = (I_m \otimes U) f$.
`Step II.` Construct block matrix D by many diagonal matrices D_{ij} in Eq. (16).
`Step III.` Solve the linear system to obtain the $\bar{\alpha}$ in Eq. (15) by separating n blocks, each one is $m \times m$ matrix equation.
`Step IV.` Recover the undetermine coefficient α by Eq. (17).

Note that in steps I, II, and IV, the fast fourier transform can be used to significantly mark up the speed of the solution process. Overall, we transform the problem for solving a large matrix system of the order $mn \times mn$ into n series of much smaller $m \times m$ system of equations. The advantages of computational efficiency is tremendous.

4 Numerical results and discussions

To demonstrate the efficiency of the algorithm using circulant matrix in the context of the BKM, four numerical examples in both 2D and 3D are given. To measure the accuracy, we define the L_2 relative error:

$$L_2 \text{ relative error} = \sqrt{\frac{\sum_{j=1}^{N_t} \left\{u(x_j) - \tilde{u}(x_j)\right\}^2}{\sum_{j=1}^{N_t} u^2(x_j)}}$$

where N_t is the total number of tested points which are randomly chosen in the computation domain, u and $\tilde{u}$ are the exact and numerical solutions respectively. All the computations were carried out on Matlab 2011b platform in OS windows 7 (32bit) with AMD 2.7GHz CPU and 3GB memory.

4.1 Two dimensional annular domain with mixed boundary conditions

We first consider a Helmholtz problem with mixed boundary conditions in two dimensional annular domain with inner radius 90 and outer radius 100 as shown in Fig. 1.

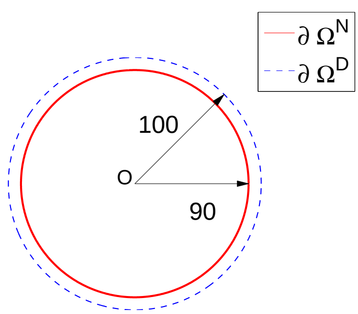

Figure 1: The profile of the two dimensional annular domain.

The problem can be described as

$$
\begin{aligned}
&(\nabla^2 + k^2)u(x,y) = 0, \qquad (x,y) \in \Omega, \\
&u(x,y) = g_d(x,y), \qquad (x,y) \in \partial\Omega_D, \\
&\frac{\partial}{\partial n}u(x,y) = g_n(x,y), \qquad (x,y) \in \partial\Omega_N,
\end{aligned}
\tag{23}
$$

where g_d and g_n are given based on the following exact solution:

$$u(x,y) = \sin\left(\frac{kx}{\sqrt{2}}\right)\cos\left(\frac{ky}{\sqrt{2}}\right).$$

Using $k = 10^3$ and $N = 2 \times 10^6$, we show in Fig. 2 the maximum absolute error at 50 test points $(r_i \cos(\pi/4), r_i \sin(\pi/4))$, where

$$r_i = 90 + \frac{10}{49}(i-1), i = 1,2,..,50.$$

In Fig. 2, we observe that high accuracy can be achieved using a large number of collocation points.

To show the impact of the number of collocation points, L_2 relative errors versus N is shown in Fig. 3 using 50 randomly distributed test points inside the annular domain. We observe that the BKM performs exceptionally well in terms of accuracy when the number of boundary points is increased. When k becomes larger, more boundary points are required to obtain the desired accuracy. Fig. 4 shows the efficiency of the circular BKM using $k = 10^3$. It is clear that the CPU time increases linearly with respect to N; i.e., $O(N)$.

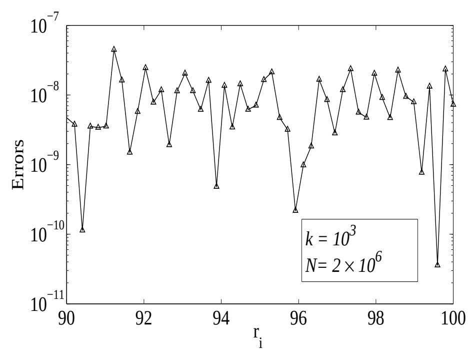

Figure 2: Maximum absolute errors distribution at test points in the annular domain.

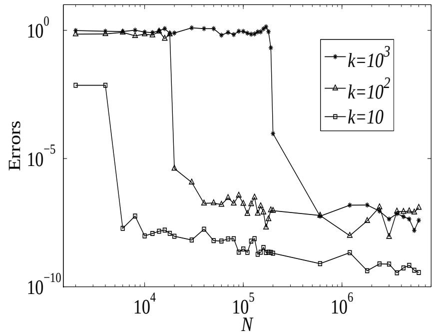

Figure 3: Errors versus the number of boundary points with different wave-number k.

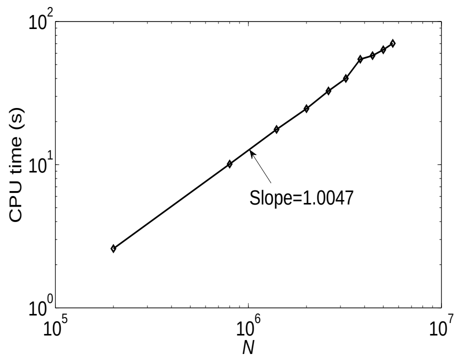

Figure 4: The number of boundary points N versus the CPU time for $k = 10^3$.

4.2 Three dimensional pulsating sphere interior problem under Neumann boundary condition

In this subsection, we consider the following interior problem in pulsating sphere (see Fig. 5)

$$\begin{aligned} &(\nabla^2 + k^2)u(\mathbf{x}) = 0, \ \ \mathbf{x} \in \Omega, \\ &\frac{\partial}{\partial n}u(\mathbf{x}) = ik, \ \ \mathbf{x} \in \partial\Omega, \end{aligned} \tag{24}$$

where k is the wave number and $\mathbf{x} = (x, y, z)$. The exact solution u at a distance from the center of the sphere is given by

$$u(r) = \frac{a}{r} \frac{ikaz_0}{ka\cos(ka) - \sin(ka)} \sin(kr), \tag{25}$$

where $r = \|\mathbf{x}\|$, a is the radius of the sphere, $z_0 = \rho_0 c_0$ is the characteristic impedance of the medium in which ρ_0 represents the density of the medium, and c_0 is the sound velocity. In the numerical implementation, we set $a = 3$ and $z_0 = 1$.

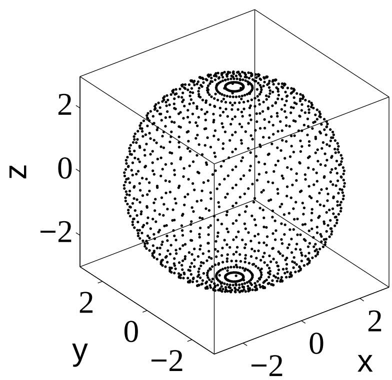

Figure 5: Three dimensional pulsating model of a sphere.

In Fig. 6 we show the number of boundary collocation points N versus L_2 relative error for various k using the circulant and traditional BKM. The traditional BKM can only handle up to 1.728×10^4 points due to the limitation of the computer memory while the circulant BKM has no problem in handling much more collocation points. For the case of high wave-number, we need much more collocation points to maintain the required accuracy. Fig. 7 shows that the circulant BKM (CBKM) is much superior than the traditional BKM for $k = 100$ in term of the efficiency.

In the spirit of reproducible research, we provide the Matlab code of this example in the Appendix. In line 7, the subroutine 'bpellipsoid' generates the boundary collocation points and the corresponding normal vectors on the surface of the sphere. In line 13, we define the derivative of general solution $\partial \psi / \partial r$ as shown in Eq. (6). In line 20, pdist2 is a Matlab function that returns a matrix DM containing the Euclidean distances between each pair of collocation points. In lines 23–27, we obtain Q in Eq. (14). In lines 29–31, $\bar{Q}$ in Eq. (15) is obtained by the fast fourier transform. In lines 33-35, the task of Eq. (21) is performed. The rest of the code is self-explanatory. For the convenience of the readers who are interested in reproducing the results in this example, the Matlab function subroutines 'CMBKM' and 'bpellipsoid' are available at the following website: www.math.usm.edu/cschen/cmbkm

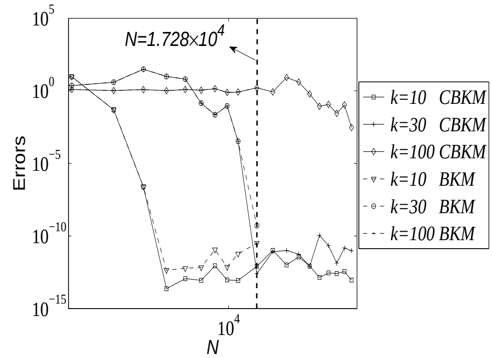

Figure 6: The number of boundary points versus L_2 relative errors with various wave-numbers for both the traditional and circulant BKM.

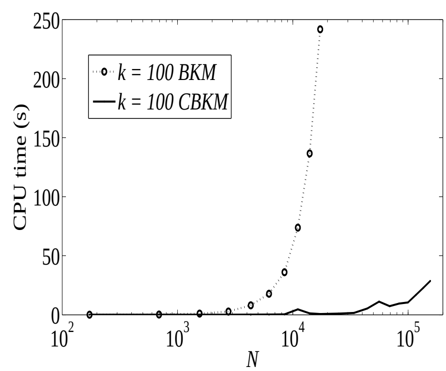

Figure 7: The number of collocation points versus CPU time for both the traditional and circulant BKM.

4.3 Basketball court simulation

In this subsection, a homogeneous Helmholtz equation with Dirichlet boundary condition in a basketball court (Fig. 8 (left)) in 3D and its revolving solid in 2D (Fig. 8 (right)) is considered as follows:

$$\begin{aligned}&(\nabla^2+k^2)u(x,y,z)=0,\ \ (x,y,z)\in\Omega,\\&u(x,y,z)=10e^{i(k_1x+k_2y+k_3z)},\ \ (x,y,z)\in\partial\Omega,\end{aligned}\tag{26}$$

where $k = \sqrt{k_1^2 + k_2^2 + k_3^2}$. The exact solution is given by

$$u(x,y,z) = 10e^{i(k_1 x + k_2 y + k_3 z)}. \tag{27}$$

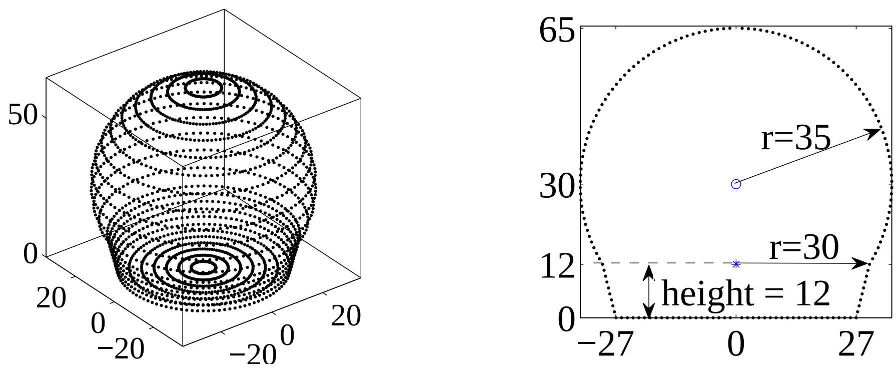

Figure 8: Profile of the basketball court in 3D (left) and 2D view (right).

In the numerical implementation, we fix $k_1 = k_2 = 0.25$, and thus k depends purely on k_3. In Fig. 9, we show the CPU time versus the number of collocation points with wave-number while $k_3 = 5\pi$, i.e. the non-dimensional wave-number $k_{non} = k \times L \approx 1.1 \times 10^3$ where

$$L = max\|\mathbf{x} - \mathbf{y}\|_2, \ \mathbf{x}, \mathbf{y} \in \partial\Omega.$$

We can obtain the solution efficiently in less than 12 seconds using 7×10^4 collocation points. In Fig. 10, we observe that the solution of the circulant BKM converges very well with respect to the number of collocation points for $k_3 = 0.1$. However, for $k_3 = 4$, much more boundary knots are required to achieve the same accuracy. For $k_3 = 7.9$, the error is still unacceptable even after using the 10^5 boundary knots. In Fig. 11, we show the real and imaginary part of the acoustic pressure at point $(1, 1, 64.9992)$. For $k_{non} < 400$, we can obtain accurate solutions but inaccurate when $k_{non} > 400$.

4.4 Three dimensional multi-connected tyre-shaped domain

In this subsection, we consider the homogeneous Helmholtz equation for the Dirichlet boundary condition in a multi-connected domain. As shown in Fig. 12, the inner and outer radius of the tyre-shaped domain are 0.3 and 0.5 respectively.

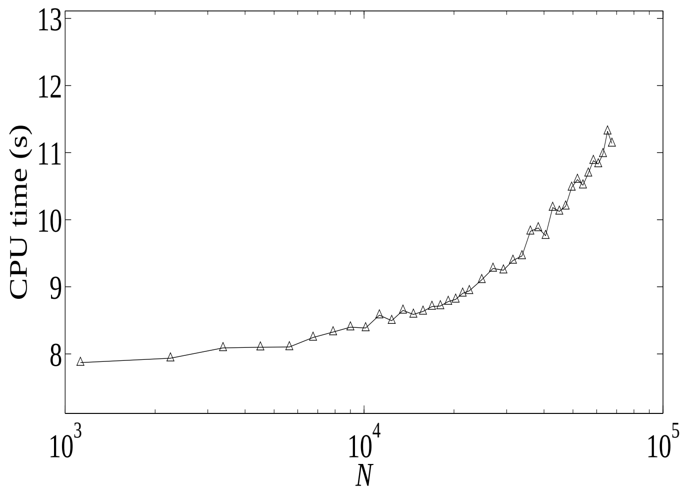

Figure 9: CPU time versus the number of collocation points with non-dimensional wave number $k_{non} \approx 1.1 \times 10^3$

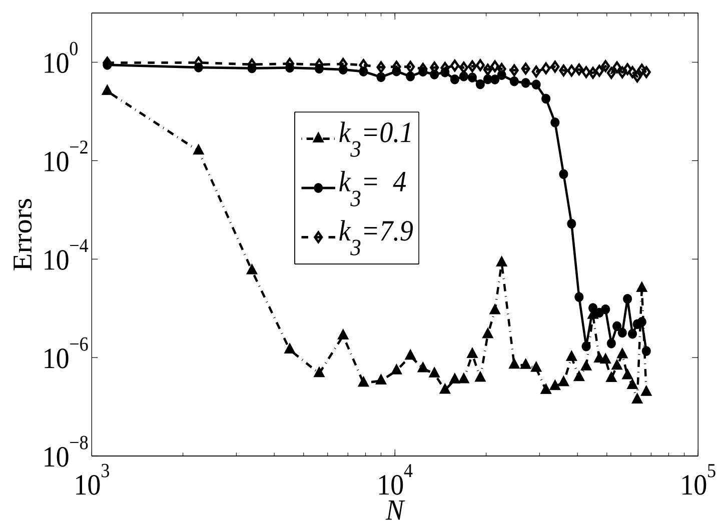

Figure 10: Errors versus the number of boundary collocation points.

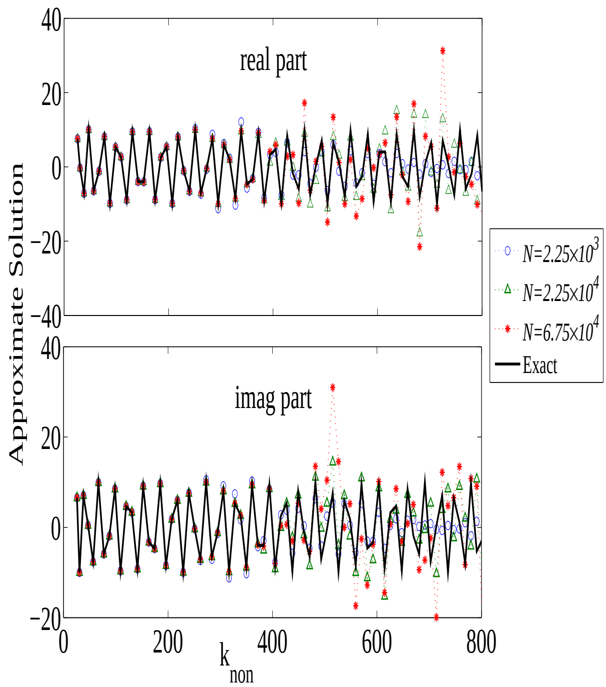

Figure 11: Numerical solution verses non-dimensional wave-number using various boundary collocation points.

The Dirichlet boundary condition is imposed based on the following exact solution

$$u(x,y,z) = \sin\left(\frac{kx}{\sqrt{3}}\right)\cos\left(\frac{ky}{\sqrt{3}}\right)\cos\left(\frac{kz}{\sqrt{3}}\right), \tag{28}$$

where k is the wave number. In the implementation, $m \times n$ circular knots are placed on the boundary which consist of m circles and n knots on each circle. In addition, 50 random test knots are selected inside the domain for the evaluation of error (see Fig. 12).

In Fig. 13, we show the accuracy verses the number of boundary points where $n = 1.2m$ for $k = 10, 100, 300$. The results shown in Fig. 14 were obtained by fixing the number of circle $m = 100$ and then increasing the number of points in each circle n for the overall number of collocation points $N = mn$. By comparing these two figures, we observe that the results obtained in Fig. 13 are more accurate than those in Fig. 14. In Fig. 15, we show the CPU time of the above two types of boundary point allocation. From above three figures, we observe that the selection of m and n has an impact on both the CPU time and accuracy.

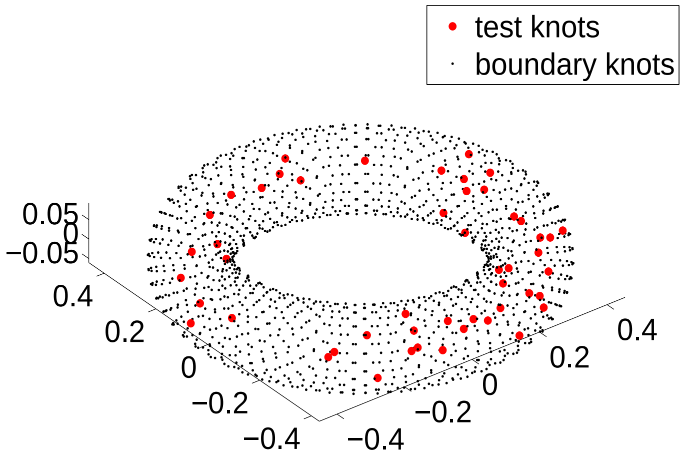

Figure 12: The profile of tyre-shaped domain.

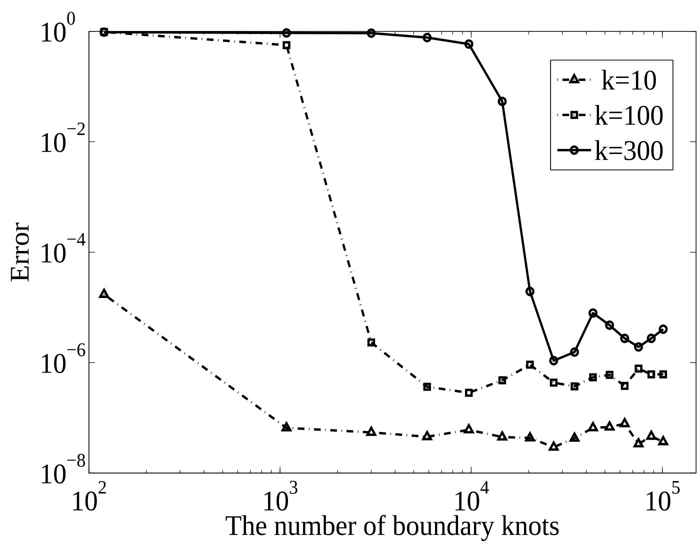

Figure 13: The accuracy of various wave numbers with respect to the number of boundary knots.

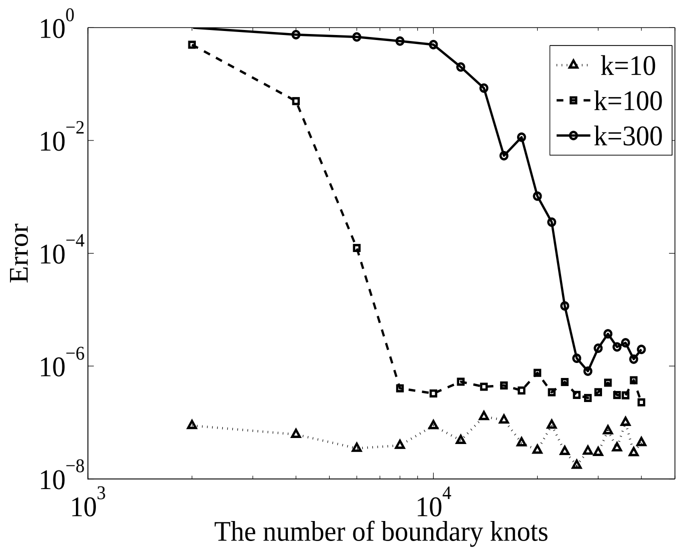

Figure 14: Error analysis by fixed the number of circles and increased the number of knot on each circle for various wave numbers *k*.

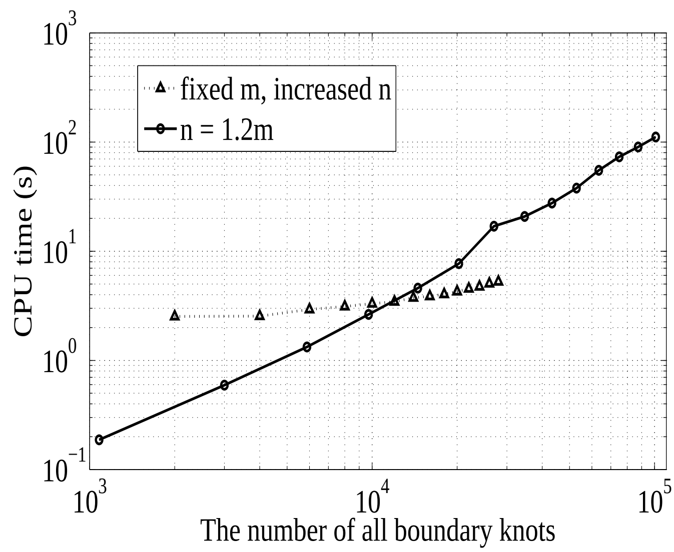

Figure 15: CPU time comparison with different knots distribution.

5 Concluding remarks

In this paper, coupled with the concept of circulant matrix, the BKM is applied to solve Helmholtz problems with high wave-numbers in axi-symmetric domains. Due to the symmetric property of the circulant matrix, a matrix decomposition algorithm is implemented to accelerate the solution process. Hence, even when a large number of collocation points is used, the computational time is still very reasonable. Coupled with radial basis functions as shown in [Karageorghis, Chen, and Smyrlis (2009)], the circulant BKM can be extended to solving inhomogeneous Helmholtz problems. The conformal mapping can also be considered in extending the axi-symmetric domain to a general domain in the 2D case. These will be the subjects of our future research.

Acknowledgement

The work described in this paper was supported by National Basic Research Program of China (973 Project No. 2010CB832702), National Science Funds for Distinguished Young Scholars (Grant No. 11125208), the R&D Special Fund for Public Welfare Industry (Hydrodynamics, Project No. 201101014 and the 111 project under grant B12032). The first author thanks the Jiangsu Province Graduate Students Research and Innovation Plan (Project no. CXZZ12_0226). The third author acknowledges the support of Distinguished Overseas Visiting Scholar Fellowship provided by the Ministry of Education of China.

Appendix

```
function  CMBKM (wn,n,m,rz,nt)
% Three dimensional pulsating sphere problem with Neumann condition
% m: # of circle on sphere;
% n: # of points on each circle;
% wn: wave number;
% rz: radius of the sphere;
% nt: number of test points.
% Generate boundary collocation points, normal vectors,
%  and random interior test points
    [xc,yc,zc,nvxc,nvyc,nvzc] = bpellipsoid(rz,rz,rz,m,n);
    theta = 2*pi*rand(nt,1); phi = rand(nt,1);
    t = rand(nt,1)*rz*2-rz; rad = sqrt(rz^2 - t.^2);
    tx =rad.*cos(theta).*phi;
    ty = rad.*sin(theta).*phi;
    tz = t .* phi;
% General solution, exact solution, Neumann condition
    GS = @(r) sin(wn*r)./r;  % General solution
```

```
    dGS = @(r) (wn*r.*cos(wn*r)-sin(wn*r))./r.^2; %Derivative of GS
    r = @(x,y,z) sqrt(x.^2+y.^2+z.^2);
    exact = @(x,y,z) 1i*rz./r(x,y,z).*wn.*rz.*sin(wn*r(x,y,z))./...
            (wn*rz*cos(rz*wn) - sin(rz*wn));  %Exact solution
    Neu = @(x,y,z) 1i*ones(size(x))*wn; %Neumann boundary condition
% DM: distance matrix;
% QM: Interpolation matrix with Neumann condition
    hat_coe = zeros(m*n,1);
    DM = pdist2([xc(1,:);yc(1,:);zc(1,:)]',[xc(:),yc(:),zc(:)]);
    pMnv = @(x,sx,nv)(repmat(x(1,:),size(x,2)*size(x,1),1) - ...
         repmat(sx(:),1,size(x,2))).*repmat(nv(1,:),...
         size(x,2)*size(x,1),1);
    QnvM = pMnv(xc,xc,nvxc) + pMnv(yc,yc,nvyc) + pMnv(zc,zc,nvzc);
    QM = dGS(DM)./DM.*QnvM.';
    for k = 1:m
        QM(k,k*n-n+1) = 0;
    end
    clear DM QnvM
    for kn = 1:m
        QM(:,kn*n-n+1:kn*n) = fft(QM(:,kn*n-n+1:kn*n),[],2);
    end
    hat_f = ifft(Neu(xc,yc,zc)).';
    for k = 1:n
        hat_coe(k:n:end) = QM(:,k:n:end) \ hat_f(:,k);
    end
    coef = fft(reshape(hat_coe,n,m));
% evaluate the approximate solution at the test points (tx,ty,tz)
    DM = pdist2([tx,ty,tz],[xc(:),yc(:),zc(:)]);
    approx = GS(DM) * coef(:);
    err = norm(approx-exact(tx,ty,tz))/norm(exact(tx,ty,tz));
    fprintf('k = %4d, m = %4d, n = %4d, error = %e\n',wn,m,n,err);
end
```

References

Alves, C. J. S.; Antunes, P. R. S. (2005): The method of fundamental solutions applied to the calculation of eigenfrequencies and eigenmodes of 2D simply connected shapes. *CMC-Computers Materials & Continua*, vol. 26, pp. 251–265.

Chen, C. S.; Cho, H. A.; Golberg, M. A. (2009): Some comments on the ill-conditioning of the method of fundamental solutions. *Engineering Analysis with Boundary Elements*, vol. 30, pp. 405–410.

Chen, W. (2002): Symmetric boundary knot method. *Engineering Analysis with Boundary Elements*, vol. 26, pp. 489–494.

Chen, W.; Hon, Y. C. (2003): Numerical investigation on convergence of boundary knot method in the analysis of homogeneous Helmholtz, modified Helmholtz and convection-diffusion problems. *Computer Methods in Applied Mechanics and Engineering*, vol. 192, pp. 1859–1875.

Chen, W.; Lin, J.; Wang, F. Z. (2011): Regularized meshless method for nonhomogeneous problems. *Engineering Analysis with Boundary Elements*, vol. 35, pp. 253–257.

Chen, W.; Tanaka, M. (2002): A meshfree, exponential convergence, integration-free, and boundary-only RBF technique. *Computers and Mathematics with Applications*, vol. 43, pp. 379–391.

Drombosky, T. W.; Meyer, A. L.; Ling, L. (2009): Applicability of the method of fundamental solutions. *Engineering Analysis with Boundary Elements*, vol. 33, pp. 637–643.

Fairweather, G.; Karageorghis, A. (1998): The method of fundamental solutions for elliptic boundary value problems. *Advances in Computational Mathematics*, vol. 9, pp. 69–95.

Fairweather, G.; Karageorghis, A.; Martin, P. A. (2003): The method of fundamental solutions for scattering and radiation problems. *Engineering Analysis with Boundary Elements*, vol. 27, pp. 759–769.

Golberg, M. A.; Chen, C. S. (Computational Mechanics Publications): *The method of fundamental solutions for potential Helmholtz and diffusion problems, in: M.A. Golberg (Ed.), Boundary Inetgral Methods-numerical and Mathematical Aspects*. Tech. Science Press.

Gu, M. H.; Young, D. L.; Fan, C. M. (2009): The Method of Fundamental Solutions for One-Dimensional Wave Equations. *CMC-Computers Materials & Continua*, vol. 11, pp. 185–208.

Hon, Y. C.; Chen, W. (2003): Boundary knot method for 2D and 3D Helmholtz and convection-diffusion problems with complicated geometry. *International Journal for Numerical Methods in Engineering*, vol. 56, pp. 1931–1948.

Jing, B. T.; Zheng, Y. (2005): Boundary knot method for some inverse problems associated with the Helmholtz equation. *International Journal for Numerical Methods in Engineering*, vol. 62, pp. 1636–1651.

Jing, B. T.; Zheng, Y. (2005): Boundary knot method for the Cauchy problem associated with the inhomogeneous Helmholtz equation. *Engineering Analysis with Boundary Elements*, vol. 29, pp. 925–935.

Karageorghis, A.; Chen, C. S.; Smyrlis, Y. S. (2009): Matrix decomposition RBF algorithm for solving 3D elliptic problems. *Engineering Analysis with Boundary Elements*, vol. 33, pp. 1368–1373.

Karageorghis, A.; Fairweather, G. (1998): The method of fundamental solutions for axisymmetric acoustic scattering and radiation problems. *Journal of the Acoustic Society of America*, vol. 104, pp. 3212–3218.

Karageorghis, A.; Fairweather, G. (1999): The method of fundamental solutions for axisymmetric potential problems. *International Journal for Numerical Methods in Engineering*, vol. 44, pp. 1653–1669.

Karageorghis, A.; Fairweather, G. (2000): The method of fundamental solutions for axisymmetric elasticity problems. *Computational Mechanics*, vol. 25, pp. 524–532.

Li, J. C.; Hon, Y. C. (2004): Domain decomposition for radial basis meshless methods. *Numerical Methods for Partial Differential Equations*, vol. 20, pp. 450–462.

Lin, C. Y.; Gu, M. H.; Young, D. L. (2010): The Time-Marching Method of Fundamental Solutions for Multi-Dimensional Telegraph Equations. *CMC-Computers Materials & Continua*, vol. 18, pp. 43–68.

Lin, J.; Chen, W.; Sze, K. Y. (2012): A new radial basis function for Helmholtz problems. *Engineering Analysis with Boundary Elements*, vol. 36, pp. 1923–1930.

Lin, J.; Chen, W.; Wang, F. Z. (2011): A new investigation into regularization techniques for the method of fundamental solutions. *Mathematics and Computers in Simulation*, vol. 81, pp. 1144–1152.

Liu, C. S. (2008): Improving the ill-conditioning of the method of fundamental solutions for 2D Laplace equation. *CMES: Computer Modeling in Engineering & Sciences*, vol. 28, pp. 77–93.

Liu, Q. G.; Sarler, B. (2013): Non-singular method of fundamental solutions for two-dimensional isotropic elasticity problems. *CMES: Computer Modeling in Engineering & Sciences*, vol. 91, pp. 235–267.

Mramor, K.; Vertnik, R.; Sarler, B. (2013): Simulation of natural convection influenced by magnetic field with explicit local radial basis function collocation method. *CMES: Computer Modeling in Engineering & Sciences*, vol. 92, pp. 327–352.

Song, R. C.; Chen, W. (2009): An investigation on the regularized meshless method for irregular domain problems. *CMES: Computer Modeling in Engineering & Sciences*, vol. 42, pp. 59–70.

Tan, F.; Zhang, Y. L.; Wang, Y. H.; Miao, Y. (2011): A meshless hybrid boundary node method for kirchhoff plate bending problems. *CMES: Computer Modeling in Engineering & Sciences*, vol. 75, pp. 1–31.

Tsangaris, T.; Smyrlis, Y. S.; Karageorghis, A. (2004): A matrix decomposition MFS algorithm for biharmonic problems in annular domains. *CMC-Computers Materials & Continua*, vol. 1, pp. 245–258.

Tsangaris, T.; Smyrlis, Y. S.; Karageorghis, A. (2006): A matrix decomposition MFS algorithm for problems in hollow axisymmetric domains. *Journal of Scientific Computing*, vol. 28, pp. 31–50.

Wang, F. Z.; Chen, W.; Jiang, X. R. (2010): Investigation of regularized techniques for boundary knot method. *International Journal for Numerical Methods in Biomedical*, vol. 26, pp. 1868–1877.

Wang, F. Z.; Ling, L.; Chen, W. (2009): Effective condition number for boundary knot method. *CMC-Computers Materials & Continua*, vol. 12, pp. 57–70.

Zhang, J. Y.; Wang, F. Z. (2012): Boundary knot method: an overview and some novel approaches. *CMES: Computer Modeling in Engineering & Sciences*, vol. 88, pp. 141–153.

Zheng, H.; Chen, W.; Zhang, C. Z. (2013): Multi-domain boundary knot method for ultra-thin coating problems. *CMES: Computer Modeling in Engineering & Sciences*, vol. 90, pp. 179–195.